

Disentangling Cooper-pair formation above T_c from the pseudogap state in the cuprates

Takeshi Kondo,¹ Yoichiro Hamaya,² Ari D. Palczewski,¹ Tsunehiro Takeuchi,^{2,3}
J. S. Wen,⁴ Z. J. Xu,⁴ Genda Gu,⁵ Jörg Schmalian,¹ and Adam Kaminski¹

¹*Ames Laboratory and Department of Physics and Astronomy,
Iowa State University, Ames, IA 50011, USA*

²*Department of Crystalline Materials Science,
Nagoya University, Nagoya 464-8603, Japan*

³*EcoTopia Science Institute, Nagoya University, Nagoya 464-8603, Japan*

⁴*Condensed Matter Physics and Materials Science Department,
Brookhaven National Laboratory, Upton, New York 11973, USA*

⁵*Condensed Matter Physics and Materials Science Department,
Brookhaven National Laboratory, Upton, New York 11973, USA*

The discovery of the pseudogap in the cuprates created significant excitement amongst physicists as it was believed to be a signature of pairing [3], in some cases well above the room temperature. In this "pre-formed pairs" scenario, the formation of pairs without quantum phase rigidity occurs below T^* . These pairs condense and develop phase coherence only below T_c [3]. In contrast, several recent experiments reported that the pseudogap and superconducting states are characterized by two different energy scales [4–7], pointing to a scenario, where the two compete [14–16]. However a number of transport, magnetic, thermodynamic and tunneling spectroscopy experiments consistently detect a signature of phase-fluctuating superconductivity above T_c [17–22] leaving open the question of whether the pseudogap is caused by pair formation or not. Here we report the discovery of a spectroscopic signature of pair formation and demonstrate that in a region of the phase diagram commonly referred to as the "pseudogap", two distinct states coexist: one that persists to an intermediate temperature T_{pair} and a second that extends up to T^* . The first state is characterized by a doping independent scaling behavior and is due to pairing above T_c , but significantly below T^* . The second state is the "proper" pseudogap - characterized by a "checker board" pattern in STM images, the absence of pair formation, and is likely linked to Mott physics of pristine CuO_2 planes. T_{pair} has a universal value around 130-150K even for materials with very different T_c , likely setting limit on highest, attainable T_c in cuprates. The observed universal scaling behavior with respect to T_{pair} indicates a breakdown of the classical picture of phase fluctuations in the cuprates.

The traditional approach of exploring the pairing origin above T_c by tracking the energy scale of spectral features has not yielded convincing results so far, as these features are poorly defined above T_c due to broad spectral peaks. The apparent smooth evolution of the spectral gap from the lowest temperatures up to T^* [1, 2, 11, 12] has previously been interpreted as key evidence for a common origin of the pseudogap and pairing gap. However, very detailed, high precision data (e. g. Fig. S3E in Supplementary Information), shows the gap size varies non-monotonically across T_c . This behavior raises doubt about the above interpretation. A better approach is to investigate the spectral weights, which are easier to quantify and in many cases interpret. A key such measure is the density of states at the Fermi energy

$D(E_F)$. In conventional, clean superconductors this weight is zero below T_c , but can be finite if there are strong impurity scattering effects. In such cases $D(E_F)$ reflects the pair breaking state. Another possibility is the case of an inhomogeneous superconductor such as cuprates [23, 24], where superconducting and "normal" patches coexist in the sample, with the latter being likely due to pair breaking states (generic density wave states, localization etc). In either case, $D(E_F)$ is proportional to the number of "normal" electrons present at E_F due to pair breaking processes. Measurements of the temperature dependence of this fundamental, yet rarely explored quantity enabled us to disentangle the electronic ground states of cuprates. Since the spectral gap in the cuprates displays significant momentum dependence, in our study we used the intensity of the spectral function at E_F , $I(E_F, k)$, which integrated over all momenta, equals $D(E_F)$ (modulo matrix elements). This approach allowed us to isolate the behavior at a specific k-point and avoid smearing due to averaging (since in general the temperature dependence of $I(E_F, k)$ will vary with momentum.)

In Fig.1a-c we examine the temperature evolution of the spectral line shape measured at the antinodal Fermi momentum in optimally doped Bi2212 ($T_c=90\text{K}$). Symmetrized EDCs[25] show the opening of pseudogap on cooling below T^* ($\sim 210\text{K}$). As the temperature is decreased below T_c , a superconducting coherent peak appears. We obtain the spectral changes with temperature by subtracting the spectrum at the highest temperature from all the spectra measured, as shown in Fig. 1b. Now we will focus on the loss of spectral weight close to the Fermi level, $W(E_F)$ (hatched area in Fig. 1b), which is due to the previously-discussed "normal" electrons. The temperature dependence of $W(E_F)$ is plotted in Fig 1d. On cooling through T^* , the spectral weight decreases linearly, which is a characteristic behavior of the pseudogap state. An astonishing feature seen in this plot is a clear deviation from the linear behavior (indicated by an arrow). Since the temperature dependence below and above this point is very different the arrow marks the onset of another distinct state. The onset temperature $T_{\text{pair}}(\sim 150\text{K})$ of this transition is considerably higher than T_c ($=90\text{K}$), but is also significantly lower than the pseudogap temperature T^* ($\sim 210\text{K}$). This state likely arises due to the pairing of the electrons because the weight loss associated with this state smoothly evolves through T_c . If we extrapolate the linear variation of $W(E_F)$ down to $T=0$, we obtain approximate values of the spectral weight lost due to pseudogap, W_{PG} (blue area) and pairing W_{pair} (red area) as marked in Fig. 1d.

We now verify this hypothesis by studying how these quantities vary with doping in

related samples of Bi2201, where T_c and T^* are more separated over a wide range of carrier concentrations [26]. The first row of Fig. 2a-g show symmetrized EDCs measured at the antinode for various temperatures and dopings from underdoped (left side) to overdoped (right side) samples. The spectral changes with temperature (obtained by subtracting the high temperature spectrum from data in panels a-g) are plotted in the panels h-n. We will focus again on the spectral weight close to the Fermi level, $W(E_F)$ (see Fig1b), which is plotted in panels o-u for all samples. As in case of Bi2212 (Fig. 1) $W(E_F)$ is linear below T^* at high temperatures, then suddenly deviates from a straight line - defining a new temperature scale T_{pair} . The temperature dependence of $W(E_F)$ evolves in a surprisingly systematic manner with doping. The linear part becomes longer with underdoping, as both T^* and T_{pair} increase. Eventually, at the lowest dopings, $W(E_F)$ is linear down to the lowest temperature, because the pseudogap completely dominates the spectra and prevents the formation of the superconducting peak at the antinode in highly underdoped samples [16]. W_{pair} decreases and W_{PG} increases with underdoping, a behavior that is consistent with the competing nature of the pairing and the pseudogap.

To validate our assertion about the pairing origin of W_{pair} , we extract this quantity for each doping by subtracting the interpolated $W_{\text{PG}}(T)$ line from each of the $W(E_F, T)$ curves and compare them in Fig. 3. Obviously the magnitude and onset temperature of W_{pair} is very different for each doping. To make a fair comparison, we rescale the vertical axis for each curve by its maximum value at $T=11\text{K}$ and horizontal axis by T_{pair} . Surprisingly the curves for all dopings fall on top of each other, demonstrating a universal scaling of W_{pair} , that smoothly evolves through T_c . This almost perfect scaling behavior not only validates our extraction of the pairing component, but it also gives compelling evidence that the pseudogap origins are not due to pairing.

We summarize our results in Fig. 4 in the form of a phase diagram, where we plot the spectral weights W_{pair} , W_{PG} using a color scale and onset temperatures of pair formation T_{pair} and the pseudogap T^* , extracted using our ARPES analysis for all dopings. We compare our data to the detection of phase-fluctuating superconductivity by magnetization[18], the Nernst effect[17] and NMR[26] as well as the pseudogap temperature extracted from resistivity measurements performed on the same samples. (see Fig. S1 of Supporting Online Material). We note the excellent agreement between these probes and ARPES. Note that ARPES reports slightly higher onset temperatures, due to fact that the other probes are sensitive to

an average over larger portions of the Fermi momenta, while with ARPES we can extract these directly for the antinodal areas only, where these temperatures are largest. The pairing temperature (T_{pair}) (panel b) increases steadily from the overdoped side of the phase diagram towards optimal doping. For dopings lower than optimal, it levels off at $\sim 130\text{K}$. This behavior contrasts to that of the pseudogap temperature (T^*) (panel c), which monotonically increases up to the lowest doping. It is quite surprising that the pairing temperature of Bi2201 is almost the same as that of Bi2212 [$\sim 150\text{K}$, see Fig. 1d], despite large difference of T_c for these two systems. This strongly suggests that, although the T_c has a significant variation for different types of cuprates, the onset temperature of pairing (130K-150K) is universal and similar to highest achievable superconducting temperature in the cuprates.

Quantitative analysis of the very detailed ARPES data presented here provides clear evidence for a spectroscopic temperature scale T_{pair} , distinct from T_c and T^* . It demonstrates that pairing and the pseudogap are two fundamentally different, coexisting and competing states. The competition between the two states plays a key role in the determination of T_c , where bulk superconductivity is established. The doping dependence of the pseudogap weight (W_{PG}), resembles that of the “checker board” pattern[28], both of them become more pronounced in the underdoped region[29] of the phase diagram. It is very likely that both the pseudogap and “checker board” pattern have a common origin and are due to an ordered state. This is strongly supported by recent STM/STS results for the same Bi2201 samples[30] as in our study, showing that the energy scale of the “checker board” pattern is almost identical over a wide range of doping with that of the pseudogap observed in our ARPES data. Our ARPES results have important consequences for understanding the mesoscale properties in the cuprates. Below T^* an ordered state emerges, that is likely a result of the underlying Mott physics and manifests itself as a “checker board” pattern [28]. Upon cooling below T_{pair} , the pairing and local superconductivity emerges at locations, where the order parameter of the pseudogap is suppressed due to impurities or defects. These superconducting inhomogeneities are observed [23], and give rise to diamagnetic[18] and Nernst [17] signals. On further cooling, the superconducting order parameter increases and an inhomogeneous superconducting state emerges in over larger and larger parts of the sample, which gives rise to an accelerated loss of spectral weight at E_F as observed in our ARPES data. Bulk superconductivity and coherent quasiparticle peaks emerge below T_c , where the pair scattering in the system is suppressed. The fact that we can observe perfect

scaling of this quantity with temperature, regardless of the impurity content and doping, implies that the only two relevant energy scales are the order parameter of the pseudogap state and the magnitude of the pairing potential, making the existence of the three temperature scales $T_c < T_{\text{pair}} < T^*$, a universal aspect of underdoped cuprates. This scaling behavior of W_{pair} gives an important clue as to the nature of the Cooper-pair fluctuations: it is not sufficient to solely consider phase fluctuations of the pairing field. T_{pair} is the temperature where the amplitude of the pairing field melts, i.e. where the strength of incoherent pairing disappears. The emergence of T_{pair} as the relevant temperature of the scaling plot requires that the pair-amplitude and phase fluctuation are equally crucial below T_{pair} . A pairing interaction that is in the extreme strong coupling limit, reminiscent of Mott physics, was shown to lead to simultaneous amplitude and pair modes that separate coherent and local pairing[27].

Methods

Optimally doped $\text{Bi}_2\text{Sr}_2\text{CaCu}_2\text{O}_{8+\delta}$ (Bi2212) single crystals with $T_c=90\text{K}$ (OP90K) and $(\text{Bi,Pb})_2(\text{Sr,L a})_2\text{CuO}_{6+\delta}$ (Bi2201) single crystals with various T_c 's were grown by the conventional floating-zone (FZ) technique. (see Supplementary Information on the sample characterization) To precisely analyze the ARPES spectra, we partially substituted Pb for Bi for all doping samples to suppress the modulation in the BiO plane, which usually contaminates the ARPES signal. ARPES data was acquired using a laboratory-based system consisting of a Scienta SES2002 electron analyzer and GammaData Helium UV lamp. All data were acquired using the HeI line with a photon energy of 21.2 eV. The angular resolution was 0.13° and $\sim 0.5^\circ$ along and perpendicular to the direction of the analyzer slits, respectively. The energy resolution was set at $\sim 10\text{meV}$ - confirmed by measuring the energy width between the 90% and 10% of the Fermi edge from the same Au reference. Custom designed refocusing optics enabled us to accumulate high statistics spectra in a short time without being affected by possible sample surface aging. In the analysis we used symmetrized EDCs normalized over the whole energy range ($-0.4\text{eV} \leq E \leq 0.4\text{eV}$) for each spectrum. We have verified that a particular normalization scheme does not affect the results of our analysis. (see Supplementary Information on the details)

Acknowledgements

We thank Andy Millis, Chandra Varma and Mike Norman for useful discussions. This work was supported by Basic Energy Sciences, US DOE. The Ames Laboratory is operated

for the US DOE by Iowa State University under Contract No. W-7405-ENG-82.

Author Contributions

T.K. and A.K. designed the experiment. T.K., Y.H., T.T., J.S.W, G.Z.J.X, and G.G grew the high-quality single crystals. T.K. and A.D.P acquired the experimental data and T.K. performed the data analysis. T.K., A.K. and J.S. wrote the manuscript. All authors discussed the results and commented on the manuscript.

-
- [1] Ding, H. *et al.* Spectroscopic evidence for a pseudogap in the normal state of underdoped high- T_c superconductors. *Nature* **382**, 51 (1996).
 - [2] Loeser, A. G. *et al.* Excitation Gap in the Normal State of Underdoped $\text{Bi}_2\text{Sr}_2\text{CaCu}_2\text{O}_{8+x}$. *Science* **273** 325-329 (1996).
 - [3] Emery, V. J. and Kivelson. S. A. Importance of phase fluctuations in superconductors with small superfluid density. *Nature* **374**, 434 (1995).
 - [4] Tanaka, K. *et al.* Distinct Fermi-Momentum-Dependent Energy Gaps in Deeply Underdoped $\text{Bi}_2\text{Sr}_2\text{CaCu}_2\text{O}_{8+x}$. *Science* **314**, 1910 (2006).
 - [5] Tacon, M. L. *et al.* Two energy scales and two distinct quasiparticle dynamics in the superconducting state of underdoped cuprates. *Nature Physics* **2**, 537 - 543 (2006).
 - [6] Kondo, T., Takeuchi, T., Kaminski, A., Tsuda, T., and Shin, S. Evidence for Two Energy Scales in the Superconducting State of Optimally Doped $(\text{Bi,Pb})_2(\text{Sr,Lu})_2\text{CuO}_{6+\delta}$. *Phys. Rev. Lett.* **98**, 267004 (2007).
 - [7] Boyer, M. C. *et al.* Imaging the two gaps of the high-temperature superconductor $\text{Bi}_2\text{Sr}_2\text{CaCu}_2\text{O}_{8+x}$. *Nature Physics* **3**, 802 - 806 (2007).
 - [8] Kanigel, A. *et al.* Evolution of the pseudogap from Fermi arcs to the nodal liquid. *Nature Physics* **2**, 447 (2006).
 - [9] Yang, H.-B. *et al.* Emergence of preformed Cooper pairs from the doped Mott insulating state in $\text{Bi}_2\text{Sr}_2\text{CaCu}_2\text{O}_{8+\delta}$. *Nature* **456**, 77 (2008).
 - [10] Wei, J. *et al.* Superconducting coherence peak in the electronic excitations of a single layer cuprate superconductor $\text{Bi}_2\text{Sr}_{1.6}\text{La}_{0.4}\text{CuO}_{6+\delta}$. *Phys. Rev. Lett.* **101**, 097005 (2008).

- [11] Meng, J. *et al.*
 Motonic d-wave superconducting gap in optimally-doped $\text{Bi}_2\text{Sr}_{1.6}\text{La}_{0.4}\text{CuO}_{6+\delta}$ superconductor
 by laser-based angle-resolved photoemission spectroscopy
 Phys. Rev. B **79**, 024514 (2009).
- [12] Nakayama, K. *et al.* Evolution of a Pairing-Induced Pseudogap from the Superconducting
 Gap of $\text{Bi}_2\text{Sr}_2\text{CuO}_{6+\delta}$. Phys. Rev. Lett. **102**, 227006 (2009).
- [13] Chatterjee, U. *et al.* Observation of a d-wave nodal liquid in highly underdoped
 $\text{Bi}_2\text{Sr}_2\text{CaCu}_2\text{O}_{8+\delta}$. Nature Physics **6**, 99 (2009).
- [14] Khasanov, R. *et al.* Evidence for competition between the superconducting and the pseudogap
 state in $(\text{BiPb})_2(\text{SrLa})_2\text{CuO}_{6+x}$ from muon-spin rotation experiments. Phys. Rev. Lett. **101**,
 227002 (2008).
- [15] Ma, J.-H. *et al.* Coexistence of competing orders with two energy gaps in real and momentum
 space in high- T_c superconductor $\text{Bi}_2\text{Sr}_{2-x}\text{La}_x\text{CuO}_{6+\delta}$. Phys. Rev. Lett. **101**, 207002 (2008).
- [16] Kondo, T., Khasanov, R., Takeuchi, T., Schmalian, J., and Kaminski, A. Competition be-
 tween the pseudogap and superconductivity in the high- T_c copper oxides. Nature **457**, 296
 (2009).
- [17] Wang, Y. *et al.* Onset of the vortexlike Nernst signal above T_c in $\text{La}_{2-x}\text{Sr}_x\text{CuO}_4$ and
 $\text{Bi}_2\text{Sr}_{2-y}\text{La}_y\text{CuO}_6$. Phys. Rev. B **64**, 224519 (2001).
- [18] Lu Li, *et al.* Diamagnetism and Cooper pairing above T_c in cuprates. Phys. Rev. B **81**, 054510
 (2010).
- [19] Corson, J., Mallozzi, R., Orenstein, J., Eckstein, J. N. and Bozovic, I. Vanishing of phase
 coherence in underdoped $\text{Bi}_2\text{Sr}_2\text{CaCu}_2\text{O}_{8+\delta}$. Nature **398**, 221 (1999).
- [20] Wang, Y. *et al.* Dependence of Upper Critical Field and Pairing Strength on Doping in
 Cuprates. Science **299**, 86 (2003).
- [21] Bergeal, N. *et al.* Pairing fluctuations in the pseudogap state of copper-oxide superconductors
 probed by the Josephson effect. Nature Physics **4**, 608 (2008).
- [22] Lee, J. *et al.* Spectroscopic Fingerprint of Phase-Incoherent Superconductivity in the Under-
 doped $\text{Bi}_2\text{Sr}_2\text{CaCu}_2\text{O}_{8+\delta}$. Science **325**, 1099 (2009).
- [23] Pan, S. H. *et al.* Microscopic electronic inhomogeneity in the high- T_c superconductor
 $\text{Bi}_2\text{Sr}_2\text{CaCu}_2\text{O}_{8+x}$. Nature **413**, 282 (2001).
- [24] Gomes, K. K. *et al.* Visualizing pair formation on the atomic scale in the high- T_c supercon-

- ductor $\text{Bi}_2\text{Sr}_2\text{CaCu}_2\text{O}_{8+\delta}$. *Nature* **447**, 569 (2007).
- [25] Norman, M. R. *et al.* Destruction of the Fermi surface in underdoped high- T_c superconductors. *Nature* **392**, 157 - 160 (1998).
- [26] Zheng, G. , Kuhns, P. L. , Reyes, A. P. , Liang, B. , and Lin. C. T. Critical Point and the Nature of the Pseudogap of Single-Layered Copper-Oxide $\text{Bi}_2\text{Sr}_{2-x}\text{La}_x\text{CuO}_{6+\delta}$ Superconductors. *Phys. Rev. Lett.* **94**, 047006 (2005).
- [27] Chubukov, A. V. and Schmalian, J. Superconductivity due to massless boson exchange in the strong-coupling limit. *Phys. Rev. B* **72**, 174520 (2005).
- [28] Hanaguri, T. *et al.* A “checkerboard” electronic crystal state in lightly hole-doped $\text{Ca}_{2-x}\text{Na}_x\text{CuO}_2\text{Cl}_2$ *Nature* **430**, 1001-1005 (2004).
- [29] Wise, W. D. *et al.* Charge-density-wave origin of cuprate checkerboard visualized by scanning tunnelling microscopy. *Nature Physics* **4**, 696-699 (2008).
- [30] Wise, W. D. *et al.* Imaging nanoscale Fermi-surface variations in an inhomogeneous superconductor. *Nature Physics* **5**, 213 (2009).

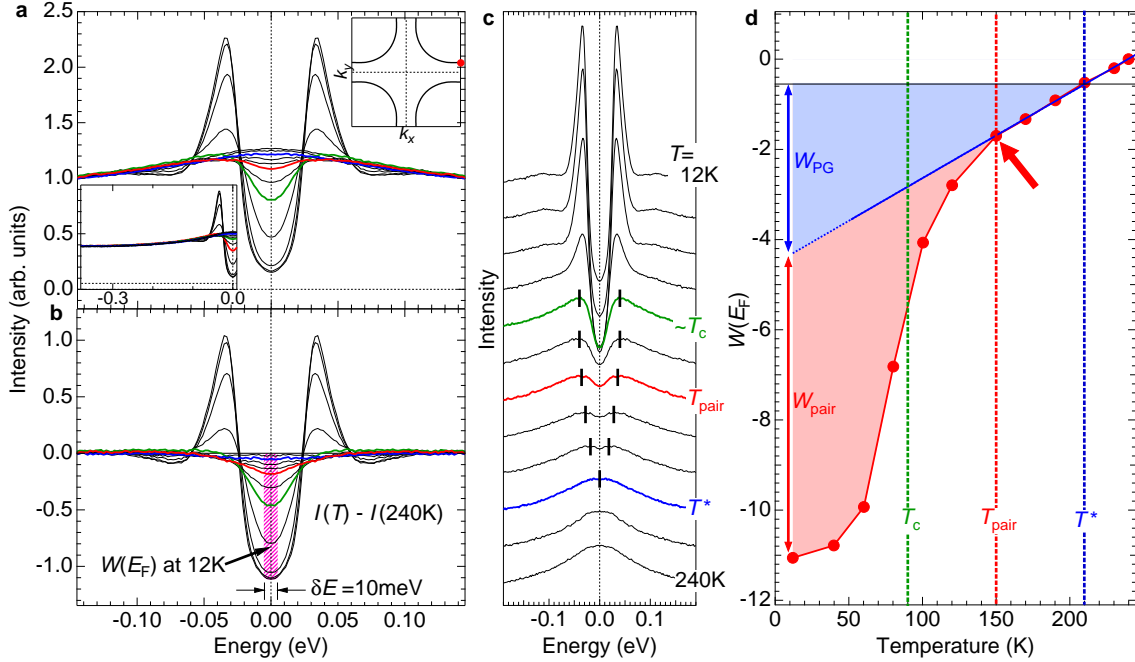


FIG. 1: Temperature dependence of the spectral weight at the chemical potential. **a** Symmetrized energy distribution curves (EDCs) [25] for various temperatures from deep below T_c to above the pseudogap temperature (T^*). The spectra were measured at the antinode in optimally doped Bi2212 ($T_c=90\text{K}$). **b** Difference spectra: the spectrum measured at the highest temperature is subtracted from each of spectra in (a). Spectral weight close to the Fermi level ($W(E_F)$, hatched area) is estimated by integrating the spectral intensity in (b) within an energy window of the experimental energy resolution (10meV). **c** Same spectra as in A with offsets. Spectral gaps are indicated with bars. **d** The temperature dependence of $W(E_F)$. The pairing temperature, T_{pair} , is defined as the onset temperature of deviation (marked by arrow) from a linear behavior seen at higher temperatures. The pseudogap temperature, T^* , is defined to be the temperature where the two spectral peaks in the symmetrized EDCs merge into a single peak as seen in (c). The three temperatures, T_c (green), T_{pair} (red), and T^* (blue) are indicated with dashed lines. The pairing weight (W_{pair} , red area) and the pseudogap weight (W_{PG} , blue area) are separated by a line extrapolated from the linear behavior of $W(E_F)$ at high temperatures.

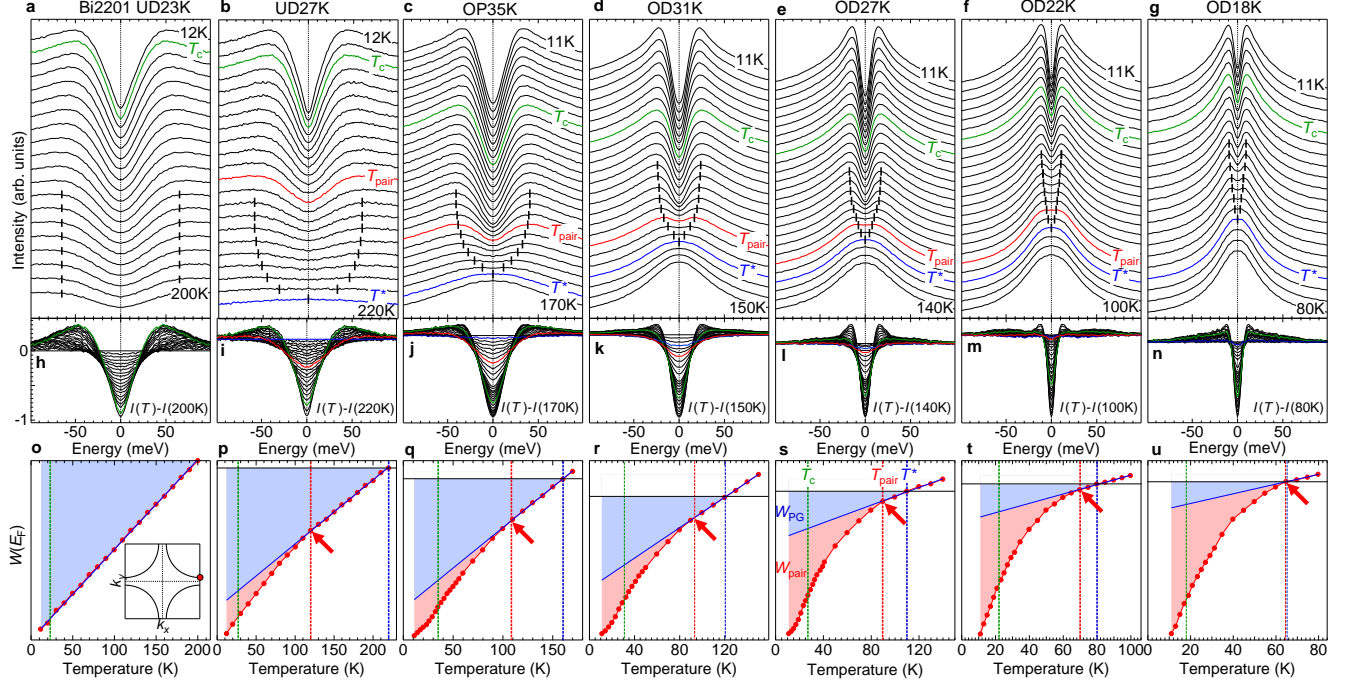


FIG. 2: Doping and temperature dependence of spectral weight at the chemical potential **a-g** Symmetrized EDCs at various temperatures measured at the antinode in Bi2201 over a wide range of doping from the underdoping (left) to overdoping (right). An offset is used for clarity. **h-n** Difference spectra: the spectrum at the highest temperature is subtracted from each of the spectra in a-g. **o-u** Temperature dependence of the spectral weight close to E_F , $W(E_F)$, obtained by integrating the spectra in k-o within the energy resolution window (10meV) about E_F . (see Fig. 1b.). The three temperatures, T_c (green), T_{pair} (red), and T^* (blue) are indicated with dashed lines. The pairing weight (W_{pair} , red area) and the pseudogap weight (W_{PG} , blue area) are separated by a line extrapolated from the linear behavior of $W(E_F)$ at high temperatures.

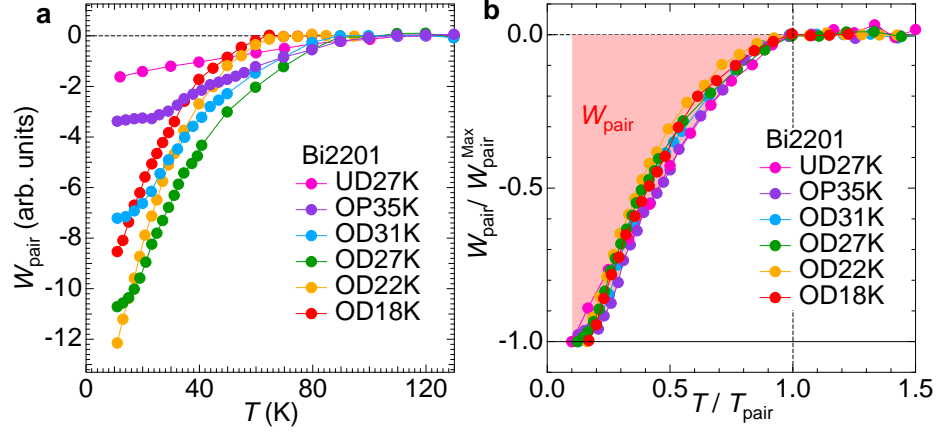


FIG. 3: Universal scaling behavior of the pairing spectral weight. **a** Temperature dependence of (W_{pair}) for all samples extracted by subtracting extrapolated W_{PG} line from $W(E_F)$ curves in Fig. 2(h-n). **b** W_{pair} from (a) scaled with the pairing temperature (T_{pair}) and the maximum value at the lowest temperature ($W_{\text{pair}}^{\text{Max}}$).

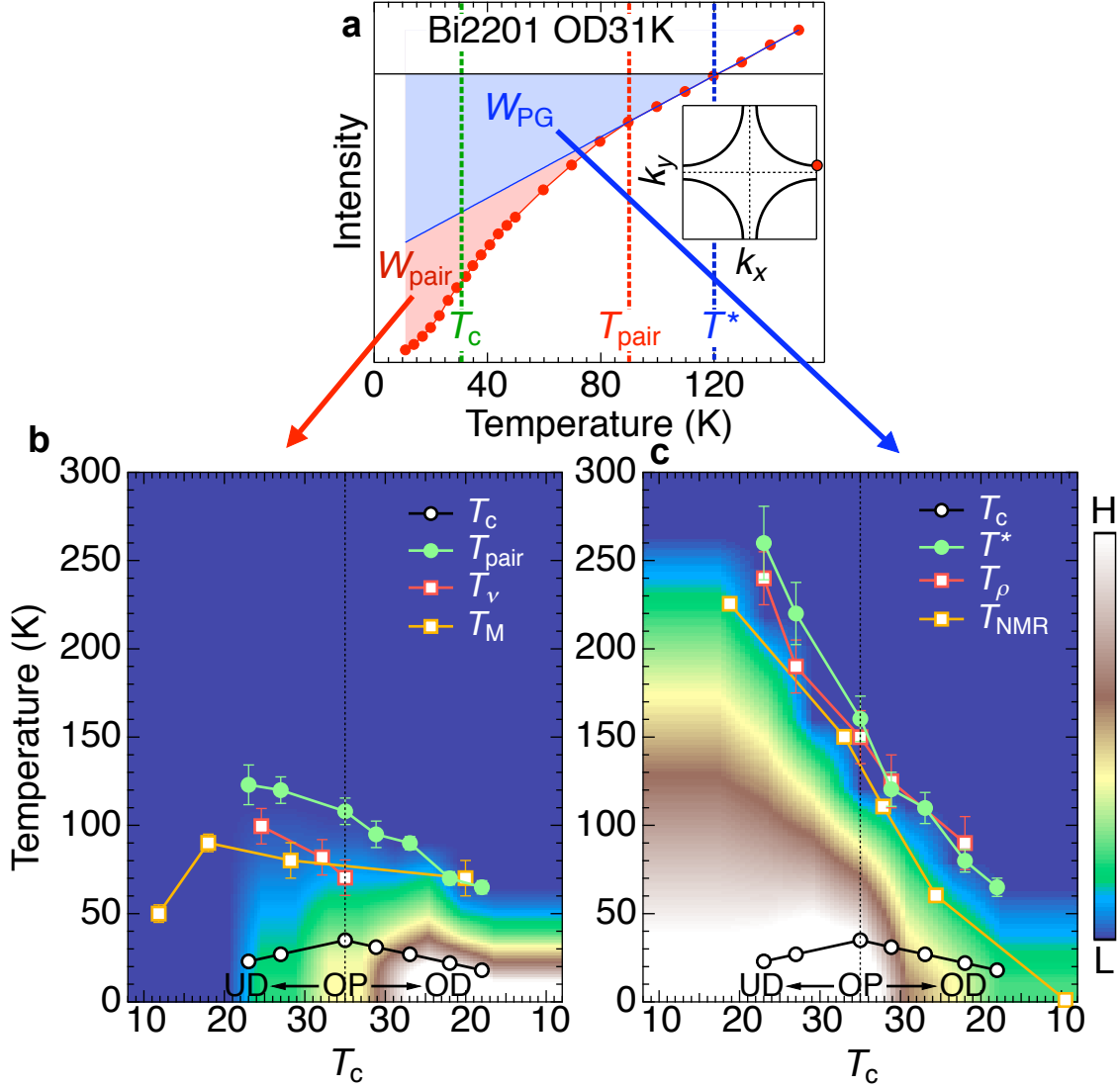


FIG. 4: Phase diagrams obtained using pairing and pseudogap spectral weights. **a** $W(E_F)$ vs T plots for OD31K, same as Fig. 2r. **b** Phase diagram obtained using the pairing spectral weight (W_{pair} , red area in a). The onset temperature of pair formation estimated from our ARPES data (T_{pair}), the onset temperature of Nernst effect (T_v) [17] and diamagnetic effect (T_M) [18] are plotted. **c** Phase diagram obtained using the pseudogap spectral weight (W_{PG} , blue area in (a)). The pseudogap temperature estimated from our ARPES data (T^*), our resistivity results (T_ρ , see Fig. S1) and NMR (T_{NMR}) [26] are plotted.

**On-line supplementary information for
Disentangling Cooper-pair formation above T_c from the
pseudogap in cuprates**

Takeshi Kondo,¹ Yoichiro Hamaya,² Ari Palczewski,¹ Tsunehiro Takeuchi,^{2,3}
J. S. Wen,⁴ G. Z. J. Xu,⁴ Genda Gu,⁴ Jörg Schmalian,¹ and Adam Kaminski¹

¹*Ames Laboratory and Department of Physics and Astronomy,
Iowa State University, Ames, IA 50011, USA*

²*Department of Crystalline Materials Science,
Nagoya University, Nagoya 464-8603, Japan*

³*EcoTopia Science Institute, Nagoya University, Nagoya 464-8603, Japan*

⁴*Condensed Matter Physics and Materials Science Department,
Brookhaven National Laboratory, Upton, New York 11973, USA*

(Dated: November 1, 2018)

I. SAMPLES

Optimally doped $\text{Bi}_2\text{Sr}_2\text{CaCu}_2\text{O}_{8+\delta}$ (Bi2212) single crystals with $T_c=90\text{K}$ (OP90K) and $(\text{Bi,Pb})_2(\text{Sr,L a})_2\text{CuO}_{6+\delta}$ (Bi2201) single crystals with various T_c 's were grown by the conventional floating-zone (FZ) technique. The carrier concentration of Bi2201 was controlled by the partial substitution of La for Sr and subsequent annealing. We obtained over-, optimally-, and underdoped samples with $T_c=18\text{K}$, 22K , 27K , 35K , 27K , and 23K (OD18K, OD22K, OD27K, OD31K, OP35K, UD27K, and UD23K), respectively. The nominal composition and annealing conditions of these Bi2201 samples are summarized in Table I.

One drawback of studying the pseudogap in high T_c cuprates such as Bi2212 is the large energy scale of superconducting gap (~ 40 meV at optimal doping), which is comparable to one of the pseudogap. This similarity makes it difficult to conclude whether or not these are separate energy scales that correspond to two different states. We chose to study Bi2201 and discuss its properties in most of this work, because Bi2201 has a low T_c of $\sim 35\text{K}$, but large T^* similar to that of Bi2212 at optimal doping, and this make it possible to investigate separately characteristics of the superconducting and pseudogap states. Bi2201 has additional advantage for our study: it is a single layered cuprate (i.e. it has a single CuO_2 plane per unit cell), therefore its spectra are free from bilayer-induced band splitting. We partially substituted Pb for Bi for all doping samples to suppress the modulation in the BiO plane, which usually contaminates the ARPES signal: the outgoing photoelectrons are diffracted, creating multiple images of the band and Fermi surface that are shifted in momentum. The bilayer-free and modulation-free samples enabled us to precisely analyze the ARPES spectra.

We measured the temperature dependence of the resistivity along the $a-b$ planes (ρ_{ab}) for OD22K, OD31K, OP35K, UD27K, and UD23K, and plot these in Fig. S1a. The signature of the pseudogap can be clearly observed in these data: resistivity is linear at high temperatures, but a change of the slope occurs at T^* . In the heavily overdoped sample OD22K, the resistivity has a T^2 component, which makes the detection of the pseudogap using above method difficult. However, the change of curvature due to the pseudogap can be easily detected examining first derivative of resistivity as demonstrated in the inset of panel a. T^* is defined as the temperature at which the slope of $d\rho_{ab}/dT$ changes. We plot T^* determined from the resistivity along with T_c for each sample in panel c. T^* obtained from the resistivity

measurements agrees well with one determined from ARPES data using “single spectral peak criterion” described in main text. Figure S1b shows magnetic susceptibility of all Bi2201 samples used in the paper. All samples show a sharp superconducting transition ($\sim 5\text{K}$).

II. EXPERIMENTAL METHOD OF ARPES

ARPES data was acquired using a laboratory-based system consisting of a Scienta SES2002 electron analyzer and GammaData Helium UV lamp. All data were acquired using the HeI line with a photon energy of 21.2 eV. The angular resolution was 0.13° and $\sim 0.5^\circ$ along and perpendicular to the direction of the analyzer slits, respectively. The energy corresponding to the chemical potential was determined from Fermi edge of polycrystalline Au reference in electrical contact with the sample. The energy resolution was set at $\sim 10\text{meV}$ - confirmed by measuring the energy width between the 90% and 10% of the Fermi edge from the same Au reference. Custom designed refocusing optics enabled us to accumulate high statistics spectra in a short time without being affected by possible sample surface aging due to absorption or loss of oxygen. Special care was taken in the purification of helium gas that supplies the UV source to remove even the smallest trace of contaminants that could contribute to surface contamination. Typically no changes in the spectral lineshape of samples were observed in consecutive measurements over several days. The samples were cooled using a closed-cycle refrigerator. Measurements were performed on several samples and we confirmed all yielded consistent results.

III. NORMALIZATION OF ARPES SPECTRA

In the analysis we used symmetrized EDCs normalized over the whole energy range ($-0.4\text{eV} \leq E \leq 0.4\text{eV}$) for each spectrum. Here we demonstrate that a particular normalization scheme does not affect the results of our analysis. In Fig. S2c, we compare four $W(E_F)$ vs T curves from a Bi2212 OP90K sample obtained with four different schemes of the normalization. First one shows the result of the spectra normalized to the total area in the range of -0.4eV to 0.4eV , as used in the the data analysis. The other three are normalized by the intensity within $\pm 30\text{meV}$ centered at -0.4eV , -0.3eV , and -0.2eV . All $W(E_F)$ vs T curves are very similar, with deviation from linear behavior occurring always at the

same temperature of $\sim 150\text{K}$. This allows us to conclude that presented results, including the determination of the pairing temperature do not depend on particular normalization scheme. We have also verified in Fig. S2d that a energy width of integration (δE , see panel b) does not significantly affect the lineshape of $W(E_F)$ vs T curves. These checks demonstrate that our analysis extracted intrinsic behavior of the low energy electronic states which is independent of details of employed analysis.

IV. SPECTRAL WEIGHT OVER A WIDE RANGE OF TEMPERATURE

In the main text, we presented the data, where the spectral weight, $W(E_F)$ displays a linear behavior even for temperatures slightly above T^* . Here we discuss the details of behavior above T^* . We also demonstrate that thanks to high quality data we can detect changes of the spectral gap across T_c , which is strong evidence supporting existence its two components. Figure S3a and b shows symmetrized EDCs plotted with and without offsets, respectively, measured over a wide range of temperatures from below T_c to far above T^* . The data were measured at the antinodal Fermi momentum for OP35K Bi2201 sample. The panel c shows the same spectra as in panel b from which data at the highest temperature was subtracted. The spectral weight close to E_F ($W(E_F)$, hatched area) is plotted in panel d as a function of temperature. As discussed in the paper, the $W(E_F)$ increases linearly from T_{pair} to slightly above T^* . At higher temperatures, the curve deviates from the straight line, and starts to decrease after reaching the maximum. We have defined T^* as a temperature at which the two peaks in symmetrized EDC merge into one peak at elevated temperature, as it is customary in the literature and which leads to T^* that agrees with one extracted from resistivity measurement. The behavior of $W(E_F)$ vs T plot in panel d indicates that the spectral weight lost due to the pseudogap state (W_{PG}) keeps filling up at E_F even slightly above the T^* , which is consistent with T^* being a cross over temperature. At higher temperatures W_{PG} saturates and eventually it starts to decrease. This is an expected behavior for metallic samples, where thermal effects became dominant and broaden the spectral peak at E_F , causing the peak height to decrease. In panel e, we plot the spectral gap (energy of the spectral peak indicated in panel a with bars) as a function of temperature. This very high quality data reveals for the first time a non-monotonic behavior; the spectral gap first increases across T_c , then decreases all the way down to zero at T^* . This characteristic

TABLE I: Sample preparation conditions for the present Bi2201 single crystals.

nominal composition	atmosphere	temperature	T_c (K)	label
$(\text{Bi}_{1.74}\text{Pb}_{0.38})\text{Sr}_{1.88}\text{CuO}_{6+\delta}$	vacuum	550C° for 24hours	18	OD18K
$(\text{Bi}_{1.74}\text{Pb}_{0.38})\text{Sr}_{1.88}\text{CuO}_{6+\delta}$	vacuum	650C° for 24hours	22	OD22K
$(\text{Bi}_{1.35}\text{Pb}_{0.85})(\text{Sr}_{1.47}\text{La}_{0.38})\text{CuO}_{6+\delta}$	Air	600C° for 24hours	27	OD27K
$(\text{Bi}_{1.35}\text{Pb}_{0.85})(\text{Sr}_{1.47}\text{La}_{0.38})\text{CuO}_{6+\delta}$	Air	450C° for 24hours	31	OD31K
$(\text{Bi}_{1.35}\text{Pb}_{0.85})(\text{Sr}_{1.47}\text{La}_{0.38})\text{CuO}_{6+\delta}$	Ar flow	650C° for 24hours	35	OP35K
$(\text{Bi}_{1.35}\text{Pb}_{0.85})(\text{Sr}_{1.40}\text{La}_{0.45})\text{CuO}_{6+\delta}$	Ar flow	650C° for 24hours	27	UD27K
$(\text{Bi}_{1.1}\text{Pb}_{1.0})(\text{Sr}_{1.28}\text{La}_{0.6})\text{CuO}_{6+\delta}$	vacuum	650C° for 24hours	23	UD23K

behavior is consistent with the existence of two different spectral components: a smaller one due to pairing below T_{pair} and a larger one due to the pseudogap state. The spectral gap is a convolution of the two energy scales and as a consequence it behaves abnormally with temperature.

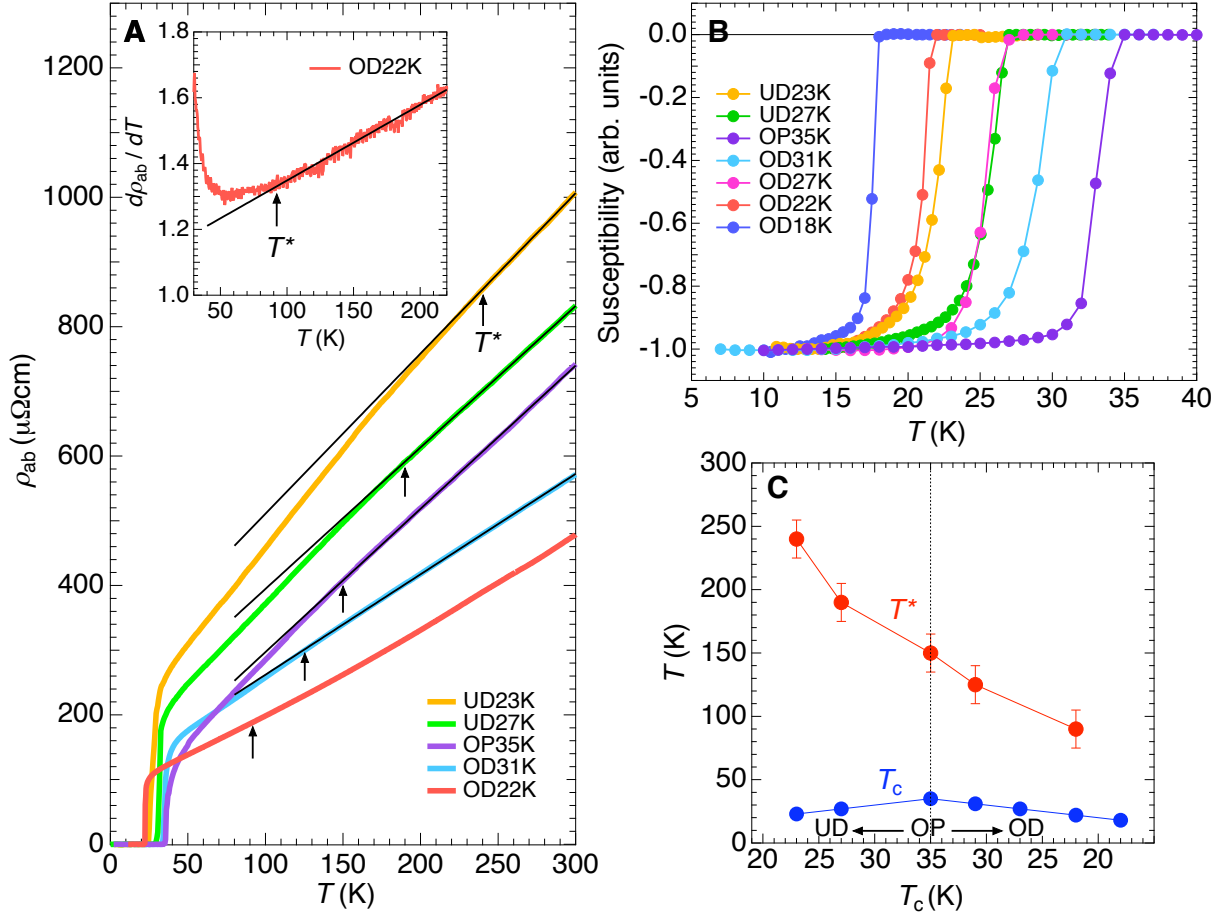


FIG. S1: Characterization of the samples using transport and susceptibility measurements. **a** Temperature dependence of resistivity along $a - b$ plane for UD23K, UD27K, OP35K, OD31K, and OD22K. Black lines are fitted to the resistivity at high temperatures. The arrow indicates the pseudogap temperature T^* defined as a temperature at which the resistivity deviates from linear behavior at high temperatures. For OD22K, T^* was estimated as a temperature at which derivative of resistivity deviates from linear behavior. **b** Magnetic susceptibility for all Bi2201 samples used in the paper. **c** Phase diagram of Bi2201. T_c and T^* are from analysis shown in panel a.

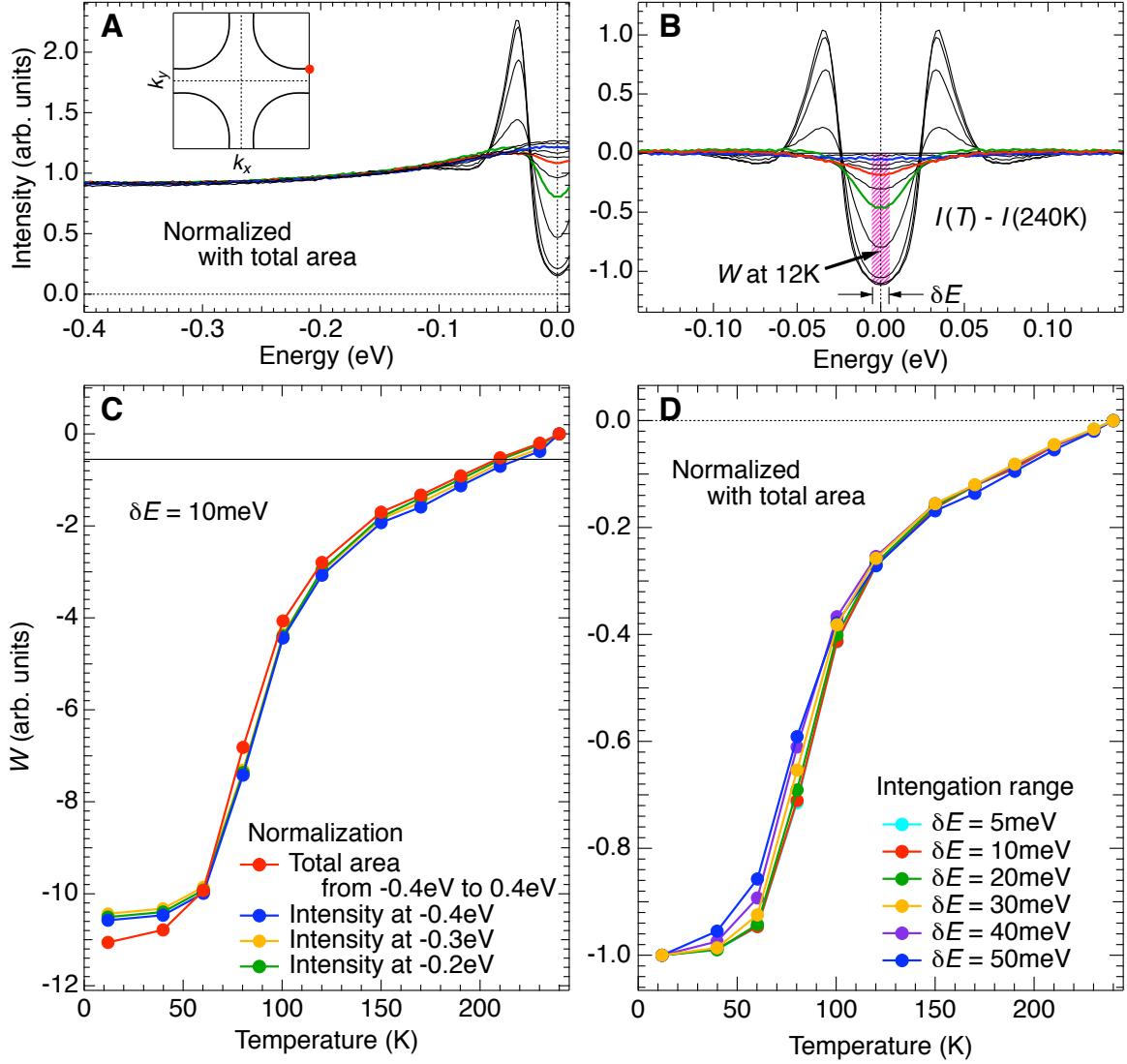


FIG. S2: Verification of normalization procedure. **a** Symmetrized EDCs at the antinodal Fermi momentum measured over a wide temperature range from below T_c to above T^* . All spectra are normalized to the total area integrated from -0.4eV to 0.4eV. **b** Same spectra as in **a** subtracted by a spectrum at the highest temperature (240K). Spectral weight at E_F , $W(E_F)$, is defined as an integrated area within an energy window of dE centered at E_F (marked as pink, hatched box). **c** Temperature dependence of $W(E_F)$ for spectra normalized using four different normalization schemes: using total area of symmetrized EDCs in range of -0.4eV to 0.4eV and normalized to the intensity within a narrow energy window ($\pm 30\text{meV}$) centered at -0.4eV, -0.3eV, and -0.1eV. **d** Temperature dependence of $W(E_F)$ calculated using different energy windows: $dE=5\text{meV}$, 10meV , 20meV , 30meV , 40meV , and 50meV centered at E_F .

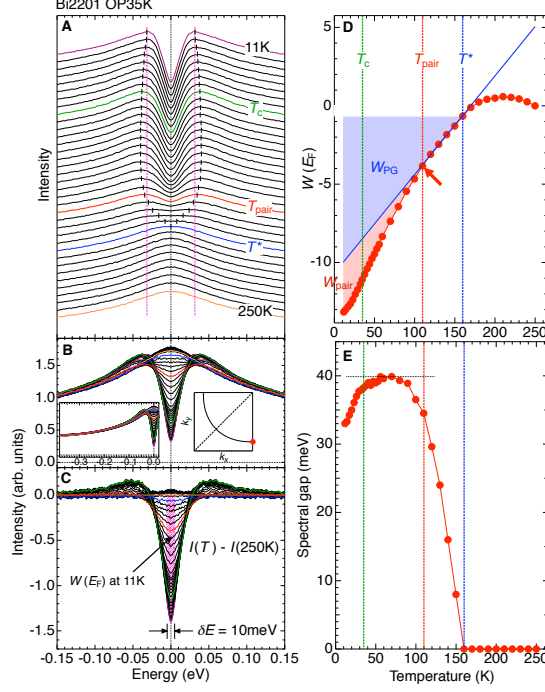


FIG. S3: **a** Energy distribution curves at various temperatures from deep below T_c to above the pseudogap closing temperature (T^*) measured at the antinodal Fermi momentum in OP35K Bi2201. All spectra are symmetrized about the Fermi level to remove the effect of the Fermi function, which cuts off the low energy intensity. Spectral gaps are indicated with bars. **b** Same spectra as in A without offsets. **c** Difference spectra: the spectrum at the highest temperature subtracted from each of spectra in b. These curves demonstrate the energy transfer of spectral weight from the high temperature. The spectral weight close to the Fermi level ($W(E_F)$) is estimated by integrating the spectral intensity in c within an energy window of the experimental energy resolution (10meV). **d** The temperature dependence of $W(E_F)$, estimated from spectra in c. The pairing temperature, T_{pair} , is defined as the onset temperature of deviation in $W(E_F)$ vs T curve from a linear behavior at higher temperatures. The pseudogap closing temperature, T^* , is defined as the temperature where the two spectral peaks in the symmetrized EDCs merge into a single peak as seen in a. Three temperatures, T_c , T_{pair} , and T^* are indicated with dashed lines. Two components of the pairing weight (W_{pair} , red area) and the pseudogap weight (W_{PG} , blue area) are separated by a line extrapolated from the linear behavior of $W(E_F)$ at high temperatures. **e** Temperature dependence of spectral gap estimated from the peak energy in symmetrized EDC (see black bars in). The maximum of the energy gap is indicated by a dotted line.